CERN/LHCC 98-20
Status Report/RD42
June 17, 1998

Development of Diamond Tracking Detectors for High Luminosity Experiments at the LHC

The RD42 Collaboration

W. Adam[1], C. Bauer[2], E. Berdermann[3], P. Bergonzo[4], F. Bogani[5], E. Borchi[6], A. Brambilla[4], M. Bruzzi[6], C. Colledani[7], J. Conway[8], W. Dabrowski[9], P. Delpierre[10], A. Deneuville[11], W. Dulinski[7], B. van Eijk[12], A. Fallou[10], F. Fizzotti[13], F. Foulon[4], M. Friedl[1], K.K. Gan[14], E. Gheeraert[11], E. Grigoriev[9], G. Hallewell[10], R. Hall-Wilton[15], S. Han[14], F. Hartjes[12], J. Hrubec[1], D. Husson[7], H. Kagan[14,◇], D. Kania[14], J. Kaplon[9], C. Karl[16], R. Kass[14], K.T. Knöpfle[2], M. Krammer[1], A. Logiudice[13], R. Lu[13], P.F. Manfredi[17], C. Manfredotti[13], R.D. Marshall[4], D. Meier[9], M. Mishina[18], A. Oh[16], L.S. Pan[14], V.G. Palmieri[19], M. Pernicka[1], A. Peitz[8], S. Pirollo[6], R. Plano[8], P. Polesello[13], S. Prawler[20], K. Pretzl[19], M. Procario[21], V. Re[17], J.L. Riester[7], S. Roe[9], D. Roff[15], A. Rudge[9], O. Runolfsson[9], J. Russ[21], S. Schnetzer[8], S. Sciortino[6], S.V. Somalwar[8], V. Speziali[17], H. Stelzer[3], R. Stone[8], B. Suter[21], R.J. Tapper[15], R. Tesarek[8], G.B. Thomson[8], M. Trawick[14], W. Trischuk[22], E. Vittone[13], A.M. Walsh[8], R. Wedenig[9], P. Weilhammer[9,◇], C. White[23], H. Ziock[24], M. Zoeller[14]

[1] *Institut für Hochenergiephysik der Österr. Akademie d. Wissenschaften, A-1050 Vienna, Austria*
[2] *MPI für Kernphysik, D-69029 Heidelberg, Germany*
[3] *GSI, Darmstadt, Germany*
[4] *LETI (CEA-Technologies Avancees) DEIN/SPE - CEA Saclay, 91191 Gif-Sur-Yvette, France*
[5] *LENS, Florence, Italy*
[6] *University of Florence, Florence, Italy*
[7] *LEPSI, IN2P3/CNRS-ULP, Strasbourg 67037, France*
[8] *Rutgers University, Piscataway, NJ 08855, U.S.A.*
[9] *CERN, CH-1211, Geneva 23, Switzerland*
[10] *CPPM, Marseille 13288, France*
[11] *LEPES, Grenoble, France*
[12] *NIKHEF, Amsterdam, Netherlands*
[13] *Univerity of Torino, Italy*
[14] *The Ohio State University, Columbus, OH 43210, U.S.A.*
[15] *Bristol University, Bristol BS8 1TL, U.K.*
[16] *II.Inst. für Exp. Physik, Hamburg, Germany*
[17] *Universita di Pavia, Dipartimento di Elettronica, 27100 Pavia, Italy*
[18] *FNAL, Batavia, U.S.A.*
[19] *Lab. für Hochenergiephysik, 3012 Bern, Switzerland*
[20] *Univ. of Melbourne, Australia*
[21] *Carnegie-Mellon University, Pittsburgh, U.S.A.*
[22] *University of Toronto, Toronto, ON M5S 1A7, Canada*
[23] *Illinois Institute of Technology, Chicago, IL 60616, U.S.A.*
[24] *Los Alamos National Laboratory, Los Alamos, NM 87545, U.S.A.*

◇ Spokespersons

Abstract

Radiation hardness, material thickness and speed of charge collection are prime concerns for tracking devices close to the interaction region in experiments at the LHC. Tracking detectors based on CVD diamond have been shown to fulfill most of these requirements. The goal of the RD42 collaboration program is to complete the development of diamond detectors for the LHC. In this report we describe the progress we have made during the last year and outline the research program we intend to pursue in the future.

Contents

1 The RD42 1997 Research Program and Milestones

During the past year RD42 has continued to improve the quality of chemical vapour deposition (CVD) diamond material for detector applications. In 1997 we developed samples with collection distances of 250 μm up from the 1996 best of 200 μm [1]. Our active feedback loop with diamond manufacturers is primarily responsible for this success.

We continue to benchmark new material with "slow" VA2 or VA3 readout electronics, which has a characteristic shaping time of 2 μs [2]. After initial selection of the best material using the benchmark process a number of particle strip detectors were prepared with both "slow" as well as "fast" analogue DMILL/SCT32A readout electronics which has a signal peaking time of 25 ns. In addition to the improvements of the collection distance we placed a large emphasis on scaling up the size of the diamond wafers and detectors which are readily available and have begun to understand the economics of scale that this would produce. As a result the first large 2×4 cm^2 strip detector was tested at the end of 1997.

Our work has proceeded on the development of pixel diamond sensors. Electronics with suitable noise and almost suitable threshold performance have recently become available to us. This coupled with the development of a number of large collection distance samples has allowed us to vigorously pursue the development of the first truly bump-bonded diamond pixel sensors. This work has has been performed in collaboration with the groups developing front end electronics for both ATLAS and CMS.

Finally, we have continued our irradiation studies of CVD diamond taking high quality diamond to doses corresponding to ten years of LHC operation. New work this year includes exposure of samples with collection distances in excess of 100 μm to proton fluences exceeding 5×10^{15} particles per cm^2 and pion fluences of up to 2×10^{15} per cm^2. We observe less than 20 % reduction in the most probable signal at these fluences, which corresponds to more than 10 years lifetime anticipated in detectors at the LHC at a radius of 4 cm.

1.1 The LHCC Milestones

At the March 1997 LHCC meeting the last RD42 renewal was approved [3]. The LHC committee suggested that the following items be included in the 1997 program:

- attain charge collection distances greater than 200 μm (7000 to 8000 e);
- pursue radiation studies;
- test ATLAS/CMS pixel structures on diamond;
- estimate the price of production material.

The referees report included additional milestones [4] listed below:

- achieve 200 μm charge collection distance on a thin substrate ($<$ 1 mm thickness) and perform irradiation measurements;
- obtain a price estimate from industry.

1.2 Summary of Milestone Progress

During the 1997 program the best samples were produced with a charge collection distance of 250 μm. This means that we obtained an average charge of $250 \times 36 = 9000$ e in response to a minimum ionizing particle. The most probable charge of the pulse height distribution is

approximately 6000 e. Most samples have a thickness in the 400 μm to 500 μm range. Results from a tracker with 50 μm strip pitch are described in the tracking section and show a nice separation of the minimum collected charge from the pedestal for minimum ionizing particles.

Our program of testing the radiation hardness of CVD diamond has advanced significantly. Firstly we have pushed our exposures with 24 GeV/c protons up to 5×10^{15} p/cm^2 as well as extending 300 MeV/c pion fluences up to 2×10^{15} π/cm^2. This work, which is detailed in the irradiation section, has begun to show where the limits of the radiation hardness of CVD diamond may lie. We observe 10 % to 20 % reduction in the most probable signals from diamond samples exposed to these fluences. As these exceed the expected fluences, for even the smallest instrumentable radii, at the LHC we are comfortable that the CVD material irradiated so far meets any reasonable radiation hardness criteria. Secondly our radiation hardness studies have tried to answer the question whether the newer, higher quality, CVD material is any less radiation tolerant than the older material. It remains for us to irradiate the highest quality (in excess of 250 μm collection distance) material over the course of the next year, since this material has only recently become available.

In order to attain a price estimate manufacturers need to move the CVD diamond growth process from a research reactor to a production plant. We are in the process of settling on a reliable set of growth parameters for the production machine. Over the course of this year the progress on growth has proceeded on two fronts. We are now consistently receiving high quality material on small (1×1 cm^2) samples. At the same time manufacturers have been studying the technological transfer of the growth process from R&D reactors (capable of producing small substrates) to production reactors that produce the larger sensor substrates we require in a cost-effective way. The quality of material from the production reactors has proceeded in rapid steps. Wafers from the first production run exceeded 140 μm collection distance; wafers from the second production run reached 190 μm collection distance. At the same time the manufacturer is gaining important experience with the operation of production reactors to produce detector quality CVD diamond. They have estimated that they will be in a position to give a first price estimate for sensor quality material produced from a production process by the end of this year. This area will remain one of our major foci in the coming year.

We have taken upon ourselves the additional milestone of producing diamond sensors which are capable of being bump-bonded and read out by the present version of ATLAS and CMS pixel electronics. We have provided practice pieces and detectors to both ATLAS and CMS groups. The first results are presented in the pixel section. We anticipate additional results shortly as the bump bonding processes are developed.

The remaining sections present details of the work summarized above.

2 Diamond Detector Preparation Work

2.1 Status of Charge Collection Distance Measured using a Source

During the past year we characterized approximately 25 new diamond samples. The measured pulse height distribution, using a ^{90}Sr source, of one of the latest samples with a 235 μm charge collection distance as-received from the manufacturer is shown in Fig. 1. To obtain this distribution we metallized the as-delivered diamond with solid electrodes on each side. The thickness of the sample is 432 μm. Operating at an electric field of 1 V/μm we observe a Landau distribution well separated from zero. For this diamond we observe a mean signal of 8500 e and a most probable signal of 6000 e. This sample has recently been remetallized, patterned as a 50 μm pitch strip detector and tested in a 100 GeV/c pion beam at CERN. The results from the beam test are in agreement with source measurements and are presented in section 3.

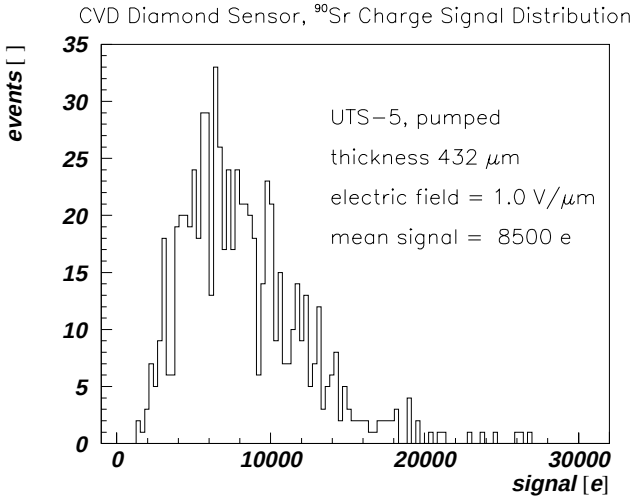

Figure 1: Charge signal distribution from a recent diamond sample measured using a ^{90}Sr source in the laboratory. No cuts to the data have been applied.

2.2 Dark Current in Diamond Detectors

Over the past few years we have characterized over 150 samples from various manufacturers. In all but a few pathological cases the dark currents observed at an electric field of 1 V/μm have been less than 1 nA/cm^2 of detector. In these measurements no guard ring is used thus the total current observed includes both the bulk current and the surface current. Fig. 2 shows a characteristic dark- and particle-induced current from a diamond sample illuminated under 37 MBq ^{90}Sr source. The dark currents observed are well below those that would add noise in either integrated charge measurements or individual *MIP*-counting.

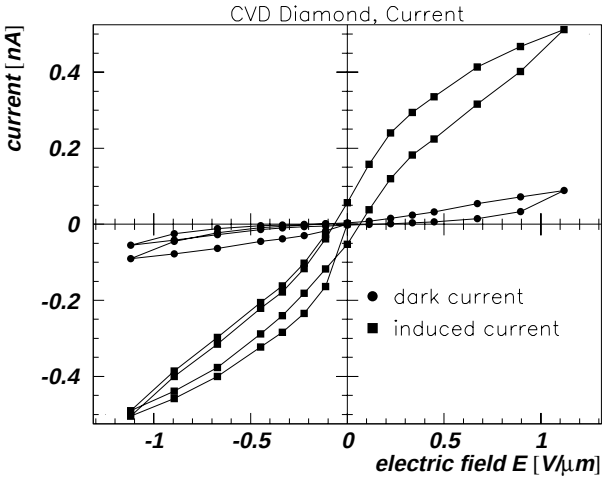

Figure 2: Dark current and particle induced current on a diamond sample measured under a ^{90}Sr source.

2.3 Contact Preparation for Diamond Detectors

In working with bump bonders for pixel detectors new metallization schemes had to be developed to make our detectors compatible with the various industrial bump-bonding processes. Our standard contacts for source measurements and strip detectors are Chromium/Gold. The Chromium is used to provide an electrical contact to the diamond. The Gold provides a non-oxidizing surface for wire bonding.

When using an Indium bonding method the preferred metallization by the bump bonders is Tungsten. We developed a Titanium/Tungsten contact which was acceptable for bump-bonding. The results of pixel electronics Indium bump-bonded to a Titanium/Tungsten diamond pixel detector are shown in section 4. We developed Chromium/Gold and Chromium/Nickel/Gold processes as well. Pixel devices with these metallizations are in the process of being bump-bonded. We have focused on these processes as a result of discussions with additional bump-bonders. The reliability of such contacts will be investigated in the coming year.

3 Results from Diamond Strip Detectors

After diamonds are sorted by the initial selection process the best diamonds are remetallized and patterned with a 50 μm pitch strip detector. Using 100 GeV/c pions it is possible to study the charge collection mechanism and spatial resolution of diamond strip detectors. Each incident pion is tracked using a silicon beam telescope to precisely predict its intersection with a diamond detector. A schematic diagram of the telescope is shown in Figure 3. The telescope has eight

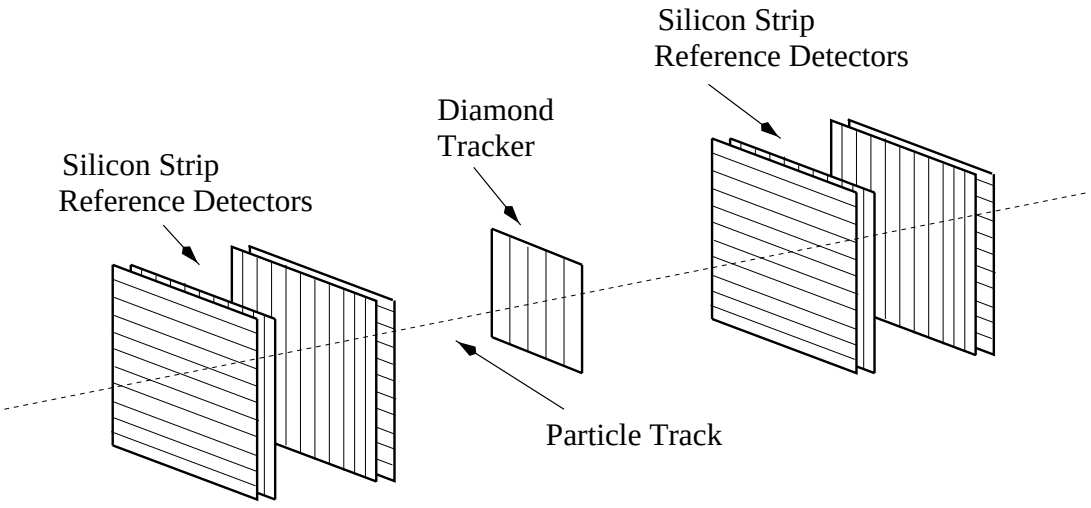

Figure 3: Schematics of the silicon beam telescope. The telescope has a lenght of 180 cm and contains eight planes of silicon strip detectors [5]. The diamond detectors under test are placed in between the two sets of planes.

planes of 50 μm pitch silicon strip detectors with floating intermediate strips arranged in two sets of four planes 180 mm apart. The silicon strip detectors are read out by VA2 chips [2]. Diamond detectors under test are placed in the region between the silicon reference planes. The position of a hit in a silicon plane is measured using an η-algorithm [6]. The difference between the measured position of a hit in a plane under test and the track fit using only the reference planes gives the residuum. The standard deviation of the residuum distribution is a meausure of the spatial resolution for that plane. The standard deviation of the residuum distribution of each silicon plane in the telescope, when excluded from the track fit, is found to be 2 μm.

Taking into account the error of the track prediction at the plane in question, we find that the intrinsic resolution of each silicon plane is approximately 1.4 μm.

Detectors under test are aligned with regard to the coordinate system of the telescope. Alignment of a detector corrects for a shift in the direction perpendicular to the strips, the tilting angle of the detector and the exact position along the beam axis. The charge signal on a strip is measured by taking the difference between the raw pulse height on this strip and the pedestal value for this strip after correcting for common mode noise. The response of a detector plane to a particle which intersects the plane is called a hit. In a *cluster analysis* this hit is found by searching the seed strip with the highest charge signal which exceeds a given signal-to-noise threshold. A hit cluster includes neighbour strips with charge signals above a given signal-to-noise threshold. The threshold for adjacent strips is typically 1/3 of the threshold which was required for the seed strip. The sum of charge signals in the hit cluster gives the hit cluster charge. The hit position is determined from an "n-strip" algorithm which calculates the pulse-height-weighted centroid. In a *transparent analysis* the pulse heights of the three closest strips to the track are used independent of any threshold or other requirements. Although this method does not introduce any threshold biases it does allow noise pulses to be added to the pulse height sum.

During the past year RD42 tested numerous diamond detectors in the X5 pion beam. We present here the results from a recent 1×1 cm^2 tracker, the first 2×4 cm^2 tracker, an initial scan of pulse height uniformity of diamonds from two manufacturers at the 100×100 μm^2 scale, and recent results with DMILL/SCT electronics.

3.1 Beam Test Results from Small Trackers

One of the best new diamonds was delivered from the manufacturer with flat substrate- and growth surfaces and a thickness of 432 μm. After source testing revealed this as a promising sample [Fig. 1], a 50 μm pitch strip detector was patterned on the diamond and it was read out by VA2 electronics. Fig. 4 shows the pulse height distribution obtained in both a cluster and a transparent analysis. Both analyses give a comparable signal distribution. In both the cluster and transparent analysis the charge signal is clearly separated from zero. The charge signal starts at one third of the most probable signal. The mean signal corresponds to 8550 e in the cluster analysis and 8100 e in the transparent analysis. These observations are consistent with the source measurement of Fig. 1 although the pulse height distribution here is slightly wider due to the clustering algorithm. The most probable signal-to-noise for this diamond in the cluster analysis was 46-to-1.

Fig. 5 shows the residuum distribution of this diamond strip detector with a gaussian fit indicating a spatial position resolution of 15.2 μm. After removing the track projection error of the reference planes we obtain the position resolution of the diamond to be 14.9 μm which is the digital resolution for a 50 μm pitch strip detector. Fig. 6 shows the pulse height measured on the strip nearest to the track as a function of the distance between this strip and the track. In this figure the central strip occupies the region from -12.5 μm to +12.5 μm, while the adjacent strips occupy the region from -37.5 μm to -50 μm and +37.5 μm to +50 μm. This figure illustrates that the pulse height on the strip is almost independent of the position of the track when the track passes through the strip. In between strips a linear relation is observed. Thus preliminary indications are that narrower strips will yield better resolution. In the coming year we will further investigate charge collection on strips using various strip widths in order to optimize the position resolution of diamond detectors.

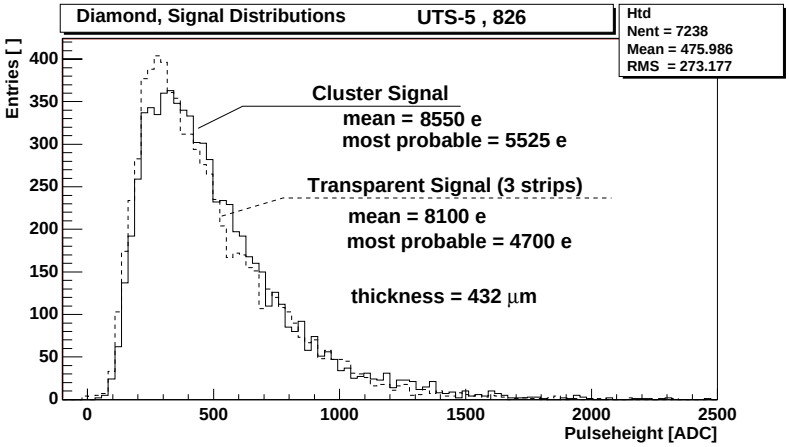

Figure 4: Distribution of charge signals measured from the diamond strip detector UTS-5. The conversion from ADC counts to electrons was measured to be 17 e/ADC.

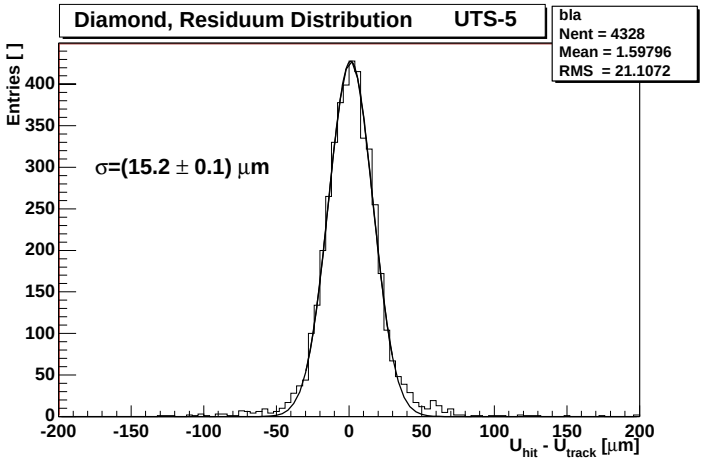

Figure 5: Distribution of residuals measured on the diamond strip detector UTS-5.

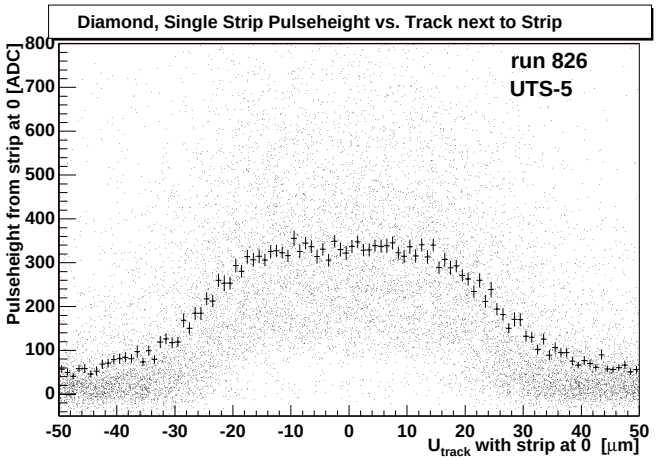

Figure 6: The signal charge distribution (dots) and its mean (crosses) measured on the strip nearest to the track as a function of the distance between the strip and the track.

3.2 Uniformity Studies

CVD diamond is inherently polycrystalline in nature. Thus one area of interest is the level of uniformity which may be achieved by various growth parameters. Ideally we would like to perform a scan on the 10 μm $\times$ 10 μm level of the entire detector surface. However a scan at this level of a 1 cm^2 diamond would take an enormous amount of data. As a result we began the study by scanning a roughly 2 $\times$ 2 mm^2 piece of diamond in 100 $\times$ 100 μm^2 bins. For a first analysis within each bin we compute the mean pulse height for three strip clusters using a *transparent* analysis.

Fig. 7 shows the preliminary results of diamonds from two manufacturers where the mean pulse height is gray scale coded. In these figures white represents no entries. A vertical white

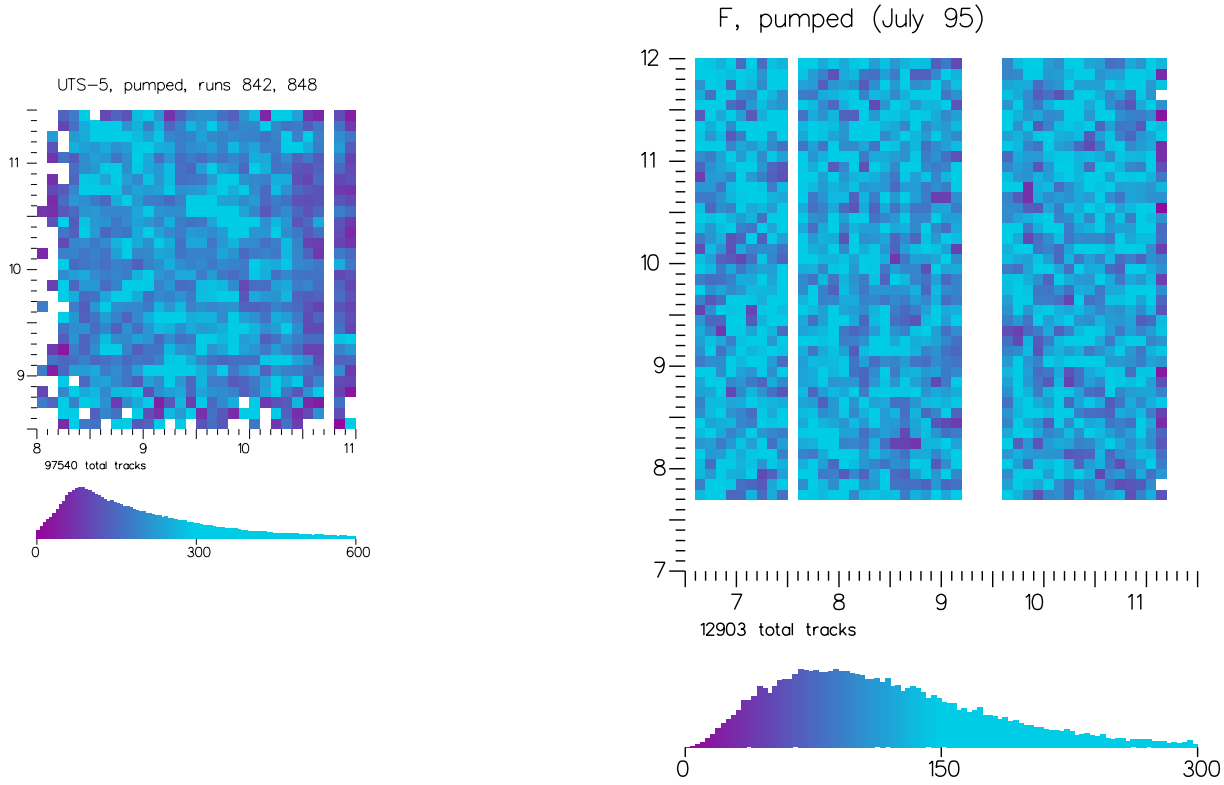

Figure 7: Mean collected charge signal versus the position of the particle track in diamonds from two different manufacturers. The size of both figures is adjusted in order to have the same number of bins per area on the printed paper.

area illustrates dead strips or dead electronics channels. respectively. The axes for these plots are the detector coodinates in real space in milimeters. We are in the process of quantifying the uniformity of such plots. Preliminary results indicate that the diamond on the right of Fig. 7 is more uniform than the one on the left. This study will continue in the coming year with more diamonds and finer bin size.

3.3 Large Area Trackers

Fig. 8 shows a photograph of the first large-area (2 $\times$ 4 cm^2) diamond strip detector with VA2 readout electronics. The diamond detector has a thickness of 650 μm and was metallized

with 3.6 cm long strips of 50 μm pitch. Producing this detector was one of the milestones for the year. The detector performed excellently. Fig. 9 shows the charge signal distribution measured on this diamond in a pion beam and several months later with a ^{90}Sr source in the laboratory for comparison. The mean value of signal distribution obtained in a transparent analysis corresponds to 5200 e and agrees with the laboratory measurement. The charge collection distance of this sample is therefore 145 μm. The spatial resolution was measured to be equal to digital resolution.

Additional 2×4 cm^2 large diamonds were delivered recently from a production reactor and are in preparation for beam tests. Measurements in the laboratory with ^{90}Sr on a tracker from that run indicate a charge collection distance of 190 μm.

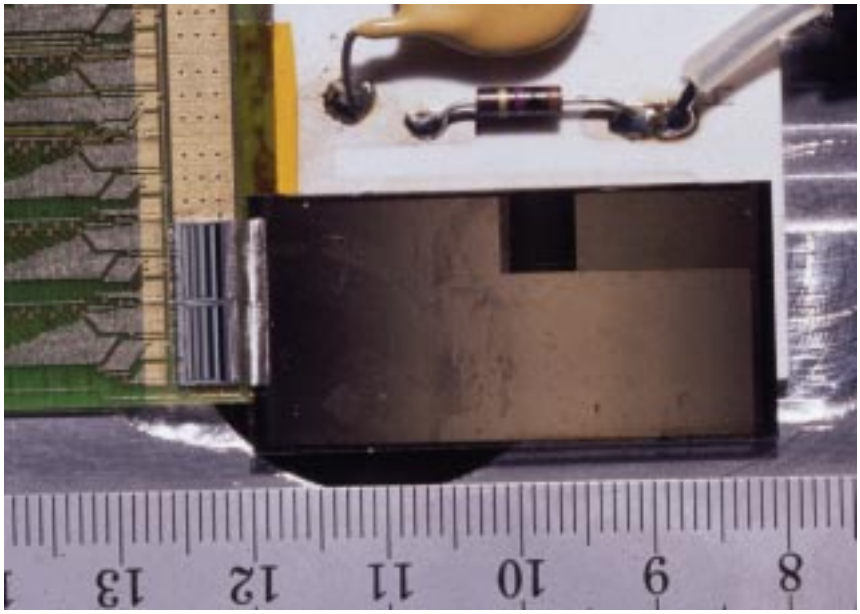

Figure 8: Photo of a large diamond tracker.

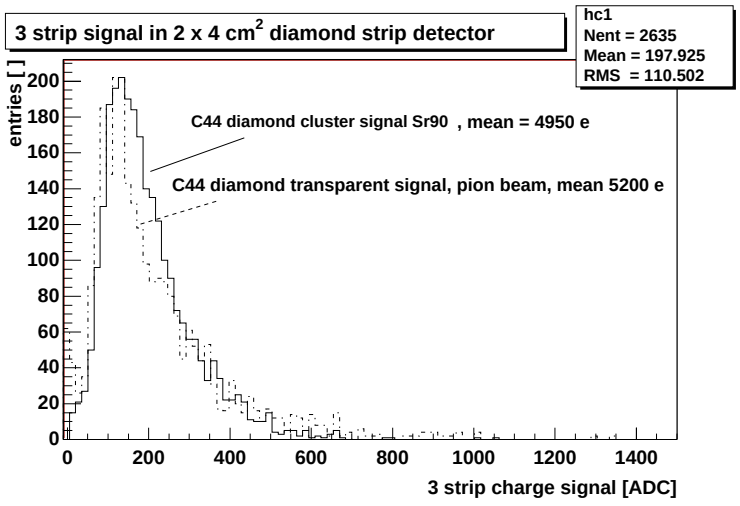

Figure 9: Charge Signal Distribution from the first large diamond strip detector.

3.4 Diamond Strip Detectors with fast SCT readout

Fast readout of diamond strip detectors was demonstrated in our last report, where we obtained a mean signal-to-noise ratio of 6-to-1 in a cluster analysis at 25 ns signal peaking time [1]. These tests have been continued with additional diamond detectors. Our goal is to demonstrate a detector/electronics combination which yields 10-to-1 most probable signal-to-noise at 25 ns signal peaking time. For the test reported here we used the 32-channel DMILL/SCT32A chip [7]. Each channel of this chip consists of a bipolar preamplifier shaper input stage followed by a 112 cell analog pipeline and a 32-channel output multiplexer. The shaper provides a signal with a peaking time of 21 to 25 ns depending on the capacitive load. The analog pipeline samples the output of the shaper at 40 MHz clock frequency. The chip is produced in radiation hard DMILL technology.

A TDC was used to measure the delay time between the trigger and clock phase for the pipeline. The mean collected charge as a function of the delay time is shown in Fig. 10. The signal has a maximum at a TDC value of about 128 ns to 134 ns. The maximum was confirmed by also measuring the signals for TDC values below 128 ns (not shown). The signal distribution obtained in a transparent analysis with a selection cut of TDC values in the time interval from 128 ns to 134 ns is shown in Fig. 11. The mean signal of the distribution is 59 ADC. The noise on a strip was measured to be 6.2 ADC which corresponds to about 750 e. The mean signal-to-noise is 10-to-1; the most probable signal-to-noise is 5-to-1. This represents a factor two improvement in signal-to-noise over the result described in our last report.

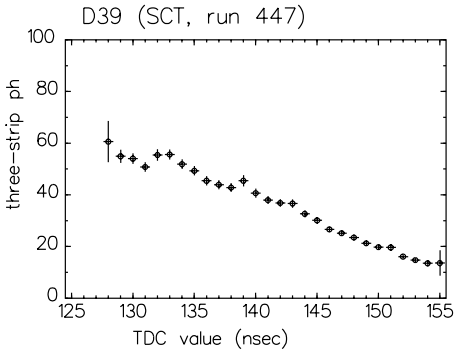

Figure 10: Transparent signal on three strips versus time difference of pipline clock phase and the trigger signal.

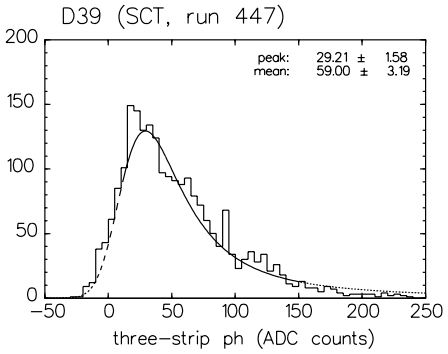

Figure 11: Distribution of charge signals measured on a diamond strip detector with DMILL/SCT32A readout.

3.5 A new fast SCT 128A Front-End chip

A follow-up version of the SCT32A chip has been designed in 1997 and was submitted to TEMIC (DMILL) in November 97 sharing an engineering run with the ATLAS SCT and LHC-B RICH projects. The design aimed at optimisation of performance for the relatively lower input capacitance of diamond detectors. The chip has now 128 channels, a pipeline with 128 cells, an input stage in each channel optimised for diamond strip detectors and a control block including power supply DACs and control and monitoring functions. The data protocol follows ATLAS specifications. Simulations predict a noise performance of ENC = 600 e to 700 e for a 6 cm long diamond strip detector. The chip has been delivered recently and is under evaluation. Full functionality of the chip has already been demonstrated. It is foreseen to test a 4 cm strip detector equipped with this chip during the summer in a test beam.

3.6 Testbeam Plans for 1998

In 1998 RD42 will test numerous tracking detectors in its three allocated beam times. The main goals of these studies will be to

- measure pulse height and resolution of the most promising samples,
- understand the effects of varying strip widths,
- study the uniformity of detector response,
- understand spatial resolution effects,
- test large-area detectors (2 cm $\times$ 4 cm), and
- continue tests of detectors with pixel and SCT electronics

4 Diamond Pixel Detectors

The first diamond pixel detector was tested in August 1996 in a particle beam [1] at CERN. This detector was read out via a wire-bonded pixel fanout structure metallized on a glass substrate. The purpose of this test was to investigate the feasibility of pixel geometries on a diamond substrate and its charge collection performance. We achieved a mean signal-to-noise ratio of 27:1 and a position resolution consistent with digital resolution for a device with 150×150 μm^2 pitch. These results were shown in last years report [1]. Based on the success of this test we produced new pixel sensors to the specifications of the high luminosity experiments, ATLAS and CMS.

Pixel detectors faciliate pattern recognition and vertexing in locations where the track occupancy in strip detectors would be too high or bulk radiation damage too great. At present both ATLAS and CMS plan to install pixel devices as the innermost layers of their tracking detector [8, 9]. Each active pixel cell will be read out by an individual charge amplifier followed by a fast shaper. The shaped signals will then be evaluated by sparsification logic and eventually delivered to the back end. The pixel detector readout chip must geometrically match the pixel pattern on the detector substrate since a single active cell on the detector substrate will be connected to its readout cell via a bump-bond. Bump-bonding is a difficult process on the 10 μm scale as is required for both experiments. Though pixel readout electronics is still in the development phase, tests have been undertaken with existing designs in order to study the bump-bonding process and contact surface treatment of the pixel sensor.

During the last year diamond pixel sensors have been prepared for true bump-bonding with the contact geometry of the diamond surface matching the requirements of the existing readout chips for ATLAS and CMS. Table 1 gives an overview of diamond sensor samples with substrate size and pixel cell size. The metallization contact and bump-bonding material are also listed.

	pixel cell size [μm^2]	diamond substrate size [μm^2]	metallization [elements]	passivation [yes/no]	bumb bonding metal
CMS	100 $\times$ 100	3725 $\times$ 4725	Cr/Au	yes	In
ATLAS/1	50 $\times$ 414.4	3800 $\times$ 5800	Cr/Ni/Au	yes	Sn/Pb
ATLAS/2	50 $\times$ 414.4	3800 $\times$ 5800	Ti/W	no	In
ATLAS/3	50 $\times$ 536	4000 $\times$ 8000	Ti/W	no	In

Table 1: Overview of diamond pixel detectors produced for pixel chips in CMS and ATLAS.

4.1 Diamond Pixel Sensors for CMS

Figure 12 shows one of the first diamond pixel sensors with a pixel metallization pattern for CMS. The pixel cells are made of Cr/Au, metallized on the diamond surface with a size of 100×100 μm^2. After annealing the Chromium forms a carbide with diamond and gives an ohmic contact to the diamond substrate. Such contact preparation is well understood from previous work on diamond strip detectors. The Chromium was covered with Gold to avoid oxidation and prepare a conductive interface for the bump-bond. The pixel cells are covered with a passivation layer. The passivation layer has a thickness of 0.2 μm and is necessary for the bump-bonding steps which follow. Figure 12 shows the result of this process. The sharp lithography gives uniform and clean pixel cells over an area of (2.1×2.9) mm^2. In the first bump-bonding tests, which were carried out at PSI in the fall of 1997, Indium was deposited from the vapour phase onto the detector surface using a metal mask with holes of 80 μm diameter. The sample was then pressed with about 1 μg/μm^2 onto a silicon substrate which was heated to 170°C. The goal is for the Indium to contract during cooling and attach itself to the pixel cell via the hole in the passivation layer. Figure 13 shows four rectangular pixel cells from the previous overview where this process succeeded. The passivation layer has a hole of about ≈ 20 μm in diameter offset in a regular pattern from each pixel center. Inside the hole the Indium pearls are attached to the gold contact of the pixel cell. The diamond surface between the pixels is not covered with the passivation layer. This preserves the high resistivity between pixel cells inherent in a diamond device, which might otherwise be compromised if a lesser insulator were present.

This process is under development at PSI. The first bump-bonding attempts yielded an Indium formation success rate of 35 % as determined by visual scan. Further test are continuing. We anticipate bump bonded detectors with CMS electronics later this year.

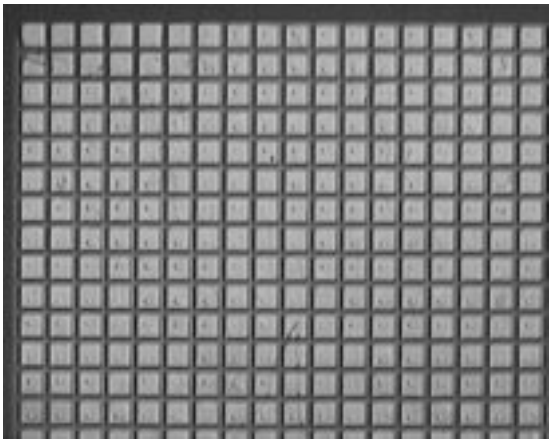

Figure 12: Top view of a CMS diamond pixel sensor showing the overall pixel pattern. The pixel metallization is Cr/Au for this device. The pixels are covered with a passivation layer. The passivation has a hole offset from the pixel center for the Indium bond.

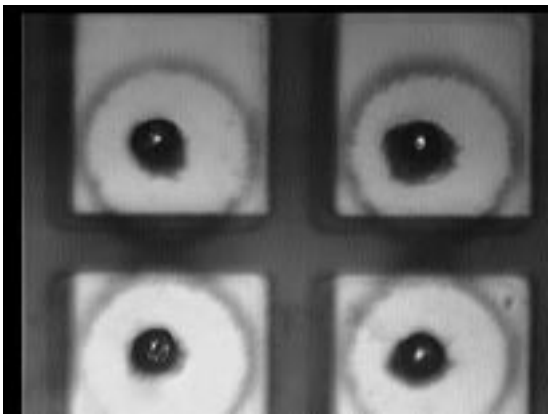

Figure 13: Four pixel cells of a CMS diamond pixel sensor. Close to the center of the pixel cells Indium pearls are visible which will form the electrical contact between the sensor and the readout chip.

4.2 Diamond Pixel Sensors for ATLAS

Three types of diamond pixel sensors were prepared with groups in ATLAS corresponding to the three types of electronics which they are prototyping.

4.2.1 Diamond Pixel Sensors for the ATLAS/1 Readout

Figure 14 shows a photo of the diamond pixel sensor which was recently prepared for the ATLAS/1 chip. This chip is an ATLAS prototype which was produced in a non-radiation-hard process. A DMILL version of it has been produced and will be be bonded to a diamond sample this summer. The pictures show the double column alignment and the bump-bond position at the end of each pixel. The sensor has a size of 3800 μm $\times$ 5800 μm and 12 columns and 63 rows of pixel cells. Each pixel cell has a size of 50 μm by 414.4 μm. The pixel metallization is made of layers of Cr/Ni/Au. The first bump-bonding trials on this sensor have been recently performed by TRONICS, using Sn/Pb solder. In this metal process the gold is melted and the solder connects to the Ni layer. Tests are underway to understand the viability of the connections achieved in this process.

Figure 14: Atlas pixel sensors: Photograph of the ATLAS/1 diamond sample with Cr/Ni/Au metallization.

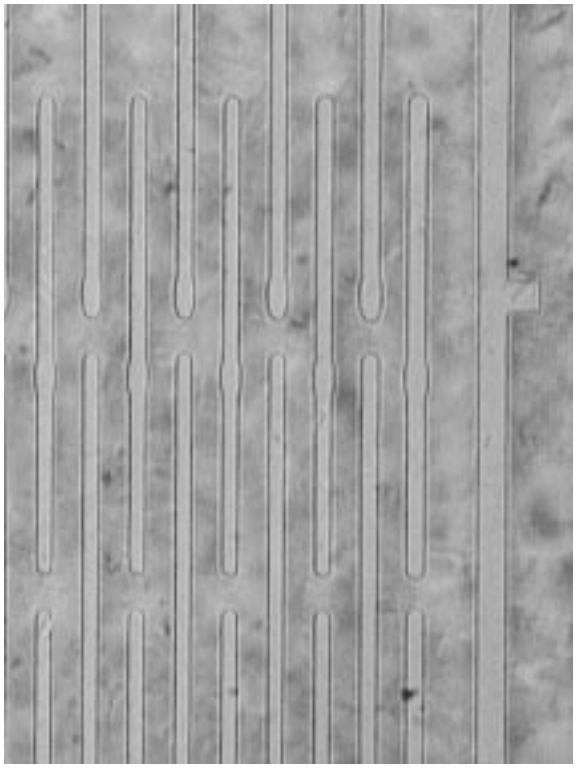

Figure 15: Atlas pixel sensors: Photograph of the ATLAS/3 diamond sensor with Ti/W metallization.

4.2.2 Diamond Pixel Sensors for the ATLAS/2 Readout

The ATLAS/2 readout chip has the same geometry as the ATLAS/1 chip. The only differnce as far as diamond prototypes are concerned is that we have prepared this detector for Indium bump-bonding. The contacts have been prepared in Ti/W (see the ATLAS/3 description below). It is anticipated that this chip will have a significantly lower threshold (as low as 1800 electrons) than any of the other chips currently available. Although it is currently only available in a non-radiation hard version the low threshold makes it particularly suitable for use with CVD diamond. We are currently negotiating with several potential Indium bump bonding vendors to have this detector assembled. The main obstacle to doing this work lies in bonding small pieces (as opposed to wafers).

4.2.3 Diamond Pixel Sensors for the ATLAS/3 Readout

The ATLAS/3 readout chip has a bricked geometry and slightly longer pixel readout cells (see table 1). The single pixel threshold can be adjusted between 3000 e and 5000 e. The chip only exists in a non-radiation hard version. Figure 15 shows the diamond pixel sensor prepared for bonding to the ATLAS/3 readout. The bricked pixel arangement, the bonding positions and part of the guard ring are visible. The diamond surface has a Ti/W metallization. The choice for Ti/W is quite natural from both the bump-bonding and the detector fabrication points of view. Ti creates the best contact with the diamond surface and faciliates the extraction of the signal, while W is an inert over-metal which is commonly used in integrated circuit processing. The size of the tracker is 4000 μm $\times$ 8000 μm, and it has 12 $\times$ 64 pixels, where every other pixel row is shifted by half of the pixel length. The pixel cells are 50 μm by 536 μm. The bricked geometry can improve the position resolution in the bricked direction by a factor of two when charge is shared between pixel cells in neighboring rows.

An ATLAS/3 pixel tracker has been produced and successfully bonded to the readout chip at Boeing. Silicon sensors previously bump-bonded by Boeing have exhibited a failure probability of less than 10^{-4} per bond. The bonding yield of the ATLAS/3 pixel tracker, as determined by visual inspection, was 100 %. We have carried out both a source and beam test with this device.

4.3 Results from the Source Test of the ATLAS/3 Pixel Detector

The ATLAS/3 tracker was tested with source at CERN in late 1997, using a ^{107}Ru beta source. The relatively low energy of the source (3.54 MeV end-point energy) meant that it was not possible to include a silicon reference plane between the pixel prototype and the trigger. Thus no external spatial information was available for this initial test. The source was mounted 5 cm from the surface of the pixel detector. A 7×7 mm^2 scintillator trigger counter was mounted 3 cm behind the pixel detector. In order to quantify the trigger acceptance and efficiencies a silicon pixel detector (readout with the same ATLAS/3 readout chip) was tested in parallel. We took about 15000 triggers in the silicon test run. We observe 5100 hits (approximately 7 hits/pixel) in the silicon pixel detector which roughly corresponds to the 35 % geometric acceptance expected from the active area of the pixel detector (17.3 mm^2) relative to the area of the trigger (49 mm^2).

During the diamond source test the threshold (4500 e) on the readout chip could not be set as low as we would have liked. Moreover the signal size of a diamond detector may be increased by about a factor of 1.6 by exposing the diamond to $<$1 kRad of ionizing radiation. In this first test we decided not to pump-up the diamond pixel detector since the readout chip was not implemented in a radiation hard technology and could have been damaged. We took about 39000 source triggers with this diamond pixel detector. However the combination of high threshold and reduced signal led us to observe about 2 hits per pixel. We conclude from this test that at least 90 % of the pixels were bonded and functioning properly. This result was sufficiently encouraging to remount this tracker in a pion testbeam at CERN.

4.4 Testbeam Results

The ATLAS/3 pixel tracker was tested in a 50 GeV pion beam at CERN in April of 1998. The standard RD42 silicon reference telescope [5] was used to provide four x and y measurements of the track, each with 2 μm precision. The resulting track extrapolations onto the plane of the diamond were better than 3 μm in each dimension, significantly better than the resolution expected from the pixel tracker. We collected 200000 tracks at normal incidence to the diamond

surface and have studied the pixel hit distribution, charge deposition and spatial correlations between the pixel tracker and the external reference telescope.

Figure 16 shows the number of hits found per pixel during this test. The size of the boxes

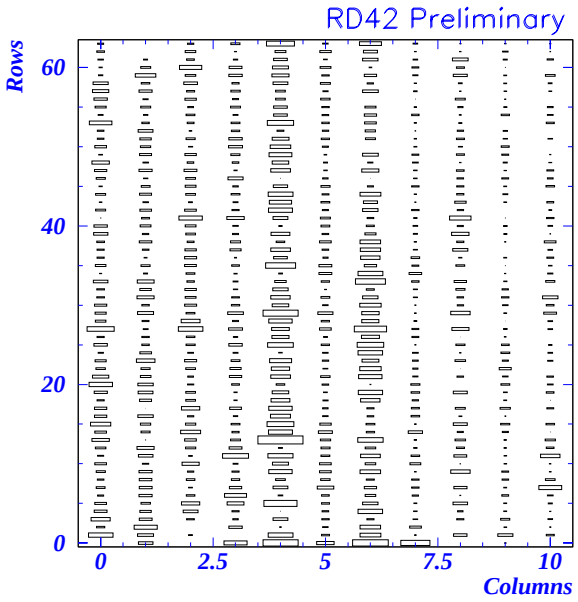

Figure 16: Number of hits per pixel seen in April 1998 testbeam.

is proportional to the number of tracks above threshold in each pixel cell. Further study of the charge distribution in columns 4 and 6 indicate that many of these hits resulted from false triggers. These columns were excluded for this initial study. In addition there is an apparent reduction in the number hits seen on the "right" half of the tracker when compared to the "left" half. This may indicate that the device was at the edge of the beam or that there was a variation of the readout threshold across the chip. This effect is still under study.

The most striking feature of Fig. 16 is that charged particle hits have been recorded in almost all of the pixel cells. This is further evidence that a high bump-bonding yield has been achieved. Figure 17 shows a projection of the number of hits seen in each pixel. In the top plot we see that there are 26 pixels that failed to record a single hit. In the lower plot we restrict our attention to the four columns on the "left" side of the tracker. There only 6 of the 256 pixels failed to record a hit. From the lower plot distribution it is clear that there is very little chance that many of these six were a fluctuation, as there is only one additional pixel which saw a single hit. From this data we conclude that at least 98 % (250/256) of the channels in this region were successfully bonded and capable of recording hits. A similar conclusion can be drawn from the top distribution. There a background subtraction, based on the number of cells with only a few hits recorded, of about 15 channels is estimated. This leaves 11 channels (26-15) that appear truly lacking hits leading us, again, to conclude that 98 % (501/512) of the channels are bonded.

Of the 200000 testbeam tracks recorded the trigger acceptance calculation predicts 66000 of them should have passed through the diamond tracker. Excluding the two noisy columns we should have seen 49000 hits. Figure 18a) shows the time-over-threshold (charge) distribution for all the tracks recorded in this run. We observe 12000 hits. We attribute this 25 % efficiency to a combination of reduced charge in the un-pumped diamond as well as a sparsification threshold of about 4000 electrons. In this testbeam we were still hesitant to expose the tracker to sufficient

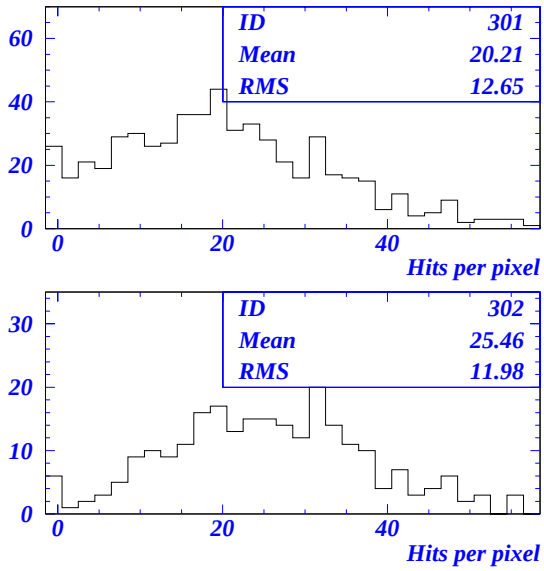

Figure 17: Distribution of number of hits per pixel cell seen in the ATLAS/3 pixel detecor. The top plot shows the distribution over the whole tracker (512 cells) while the bottom plot shows the number of hits per cell only on the "left" side of the detector.

ionising radiation to fully pump the detector.

One of the features of using diamond as a sensor material is that it can be recycled. In this case, the diamond material that we are now using as a pixel tracker was previously tested as a strip tracker. As such we have data on the charge distribution we expect from the pixel detector. The diamond used had an unpumped charge collection distance of 130 μm. Figure 18b) summarises our understanding of the situation. The solid gray histogram is the single-strip charge observed in this diamond material when it was a strip tracker with 50 μm pitch. The single strip charge is all that is relevant to our pixel tracker as we expect, and see, no significant sharing of cluster charge between neighbouring pixels. This data was taken with the tracker fully pumped. Thus, the open histogram is the single strip data scaled down by 40 % – our prediction for the signal expected from this sample in the un-pumped state. Overlaid (in black) is the actual charge observed in the pixel detector. We conclude that we were operating the tracker with a 4000 e threshold and see that such a threshold explains the missing hits.

In future tests we plan to pump-up the detector (returning to the charge distribution shown in gray in fig. 18b). If we can also lower the threshold to 2000 e then we would expect this pixel tracker to achieve an efficiency of >85 %. To move much beyond this will require a slightly lower threshold and/or higher quality diamond. We expect that in the next 12 months we will have both.

Only 20 % of the total event sample has been analyzed to provide track information at this stage. Figures 19a) and 19b) show the difference between the track positions measured by the pixel detector and the prediction of the silicon reference telescope. The resolution along the direction of the large pixel dimension (536 μm in length) is, as expected, a top-hat distribution with a full width at half maximum of about 500 μm.

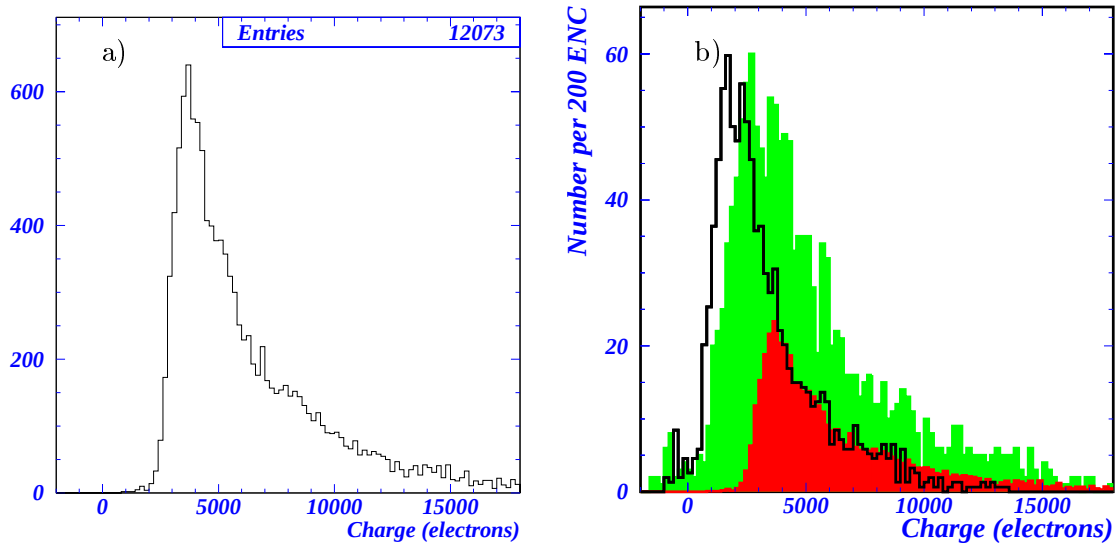

Figure 18: a) Distribution of time over threshold (charge) measurements for triggered pixels in April 1998 testbeam. b) Comparison of the charge observed in the pixel tracker (dark gray histogram) in the April 1998 testbeam with that seen in the same diamond when it was instrumented as a strip tracker in May 1997 (light gray histogram). The open histogram is a prediction, based on the observed (light gray) charge and the fact that the diamond was not pumped in the 1998 test, for the charge we should expect to see in the pixel tracker.

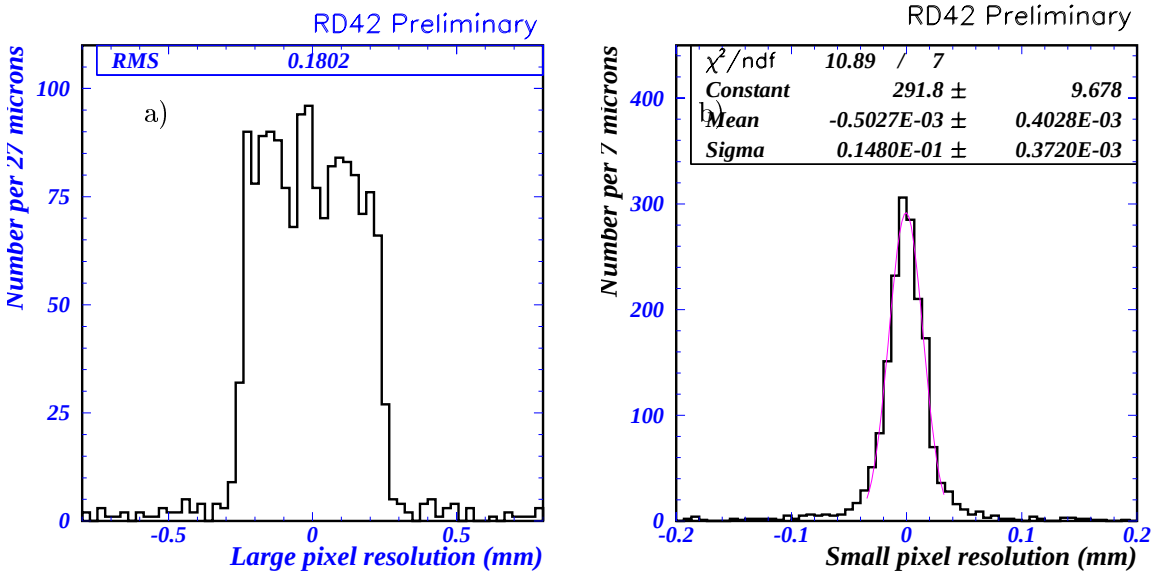

Figure 19: The position resolution of the pixel detector prototype in a) the x (long pixel) view and b) the y (short pixel) view.

In the direction measured by the small pixel dimension we see a position resolution, 14.8 μm,

consistent with the strip pitch divided by the square root of twelve. In both cases there are minimal tails beyond the main peak indicating that very few of the hits recorded by the pixel tracker are unrelated to the charged tracks measured in the telescope. It should be clear that the vast majority (over 99 %) of the hits that trigger the pixel readout chip result from the passage of charged particles also reconstructed in the reference telescope.

Work with a single prototype pixel tracker system (the ATLAS/3) has yielded a fully functional prototype that has proven high bump-bonding yields are possible. The next generation of pixel detectors will use the newly available large collection distance material (charge collection distance of 250 μm as shown in Fig. 1) and should yield a fully functional pixel detector with $\geq$99 % efficiency.

5 Irradiation Studies of CVD Diamond Sensors

Radiation hardness is crucial for particle detectors in LHC experiments. Solid state tracking detectors in the inner most layers have to resist high particle fluences to keep the charge signal-to-noise ratio above 10-to-1 after irradiation. The consequences of high radiation dose and damage in silicon devices are well known. On the one hand the leakage current increases leading to an increased noise; on the other hand fewer charges are collected due to trapping. As a result the signal-to-noise ratio in damaged detectors decreases rapidly. It has been shown in the past that CVD diamond is resistant to electromagnetically interacting radiation like photons or electrons up to 10 MRad [10] and 100 MRad [11] respectively. No decrease in charge collection distance was observed. In fact the opposite, a linear increase of charge collection distance between 0 and $<$1 kRad absorbed dose and a saturation at $<$10 kRad, has been measured. The saturation value is known as the pumped state of the diamond, which is generally higher by a factor of 1.6 to 1.9 than the depumped state.

5.1 Irradiation Studies 1997

Irradiations with protons, pions and neutrons have been carried out over the last years and were continued in 1997 with previously irradiated samples and with new samples from recent growths and higher charge collection distance. Most irradiated samples had a thickness of less than 700 μm. The recent irradiations included diamond samples with charge collection distances above 100 μm.

5.1.1 Proton Irradiation

In June 1997 diamond samples were irradiated at the Proton Synchrotron, PS, at CERN with a final fluence of 5×10^{15} p/cm^2 [12]. All samples were irradiated at room temperature and kept at 100 V. The protons had a momentum of 24.2 GeV/c. The average proton flux was 2.9×10^{10} p/cm^2/spill. The absolute proton fluence was measured using an aluminum foil activation method. Fig. 20 shows the fluence reached on each sample. After 60 hours the number of particle extractions was increased to three spills per 14 s cycle. One sample received the highest fluence of 5×10^{15} p/cm^2.

Fig. 21 shows the signal charge distribution on a diamond sample before irradiation, after 0.9×10^{15} p/cm^2 and after 5×10^{15} p/cm^2. The sample was measured in its electron pumped state before irradiation and in the proton pumped state after irradiation. Pumping occurs at relatively low dose *e.g.* from ^{90}Sr during a measurement of charge collection distance and during proton beam exposure. The charge distributions are fit by a convolution of Landau's energy loss distribution function for thin detectors and a Gaussian associated with the noise. The most

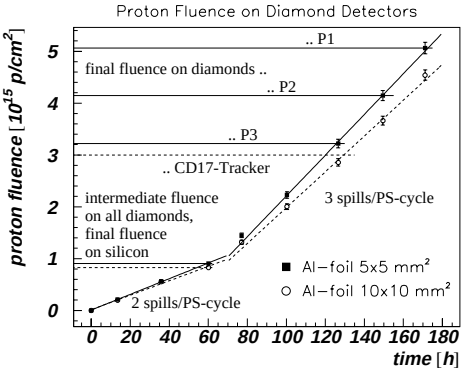

Figure 20: Proton fluence on diamond samples as a function of time up to 5×10^{15} p/cm^2. The proton fluence was measured every 20 hours using Al-foils. Two curves are shown which were measured using foils of different size. They differ slightly since the proton beam has its highest intensity in the center. The slope of the fluence increases above 70 hours since the extraction changed from 2 to 3 spills per cycle. The graph shows the final fluences reached on each sample.

probable charge signal, corresponding to the peak of the fit curve, and the mean signal increase slightly after a dose of 0.9×10^{15} p/cm^2 compared to before irradiation. After the highest fluence of 5×10^{15} p/cm^2 the most probable charge signal has decreased by 20 % compared to its pumped value from before irradiation, while the mean value decreased by about 40 % due to fewer events with high charge signal in the Landau tail.

Fig. 22 shows the relative charge collection distance as a function of proton fluence. After

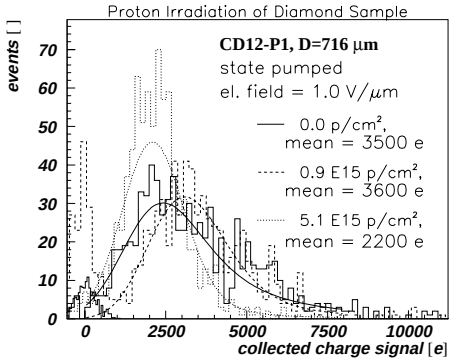

Figure 21: Charge signal distribution on a diamond sample at 1 V/μm before proton irradiation and after 5×10^{15} p/cm^2.

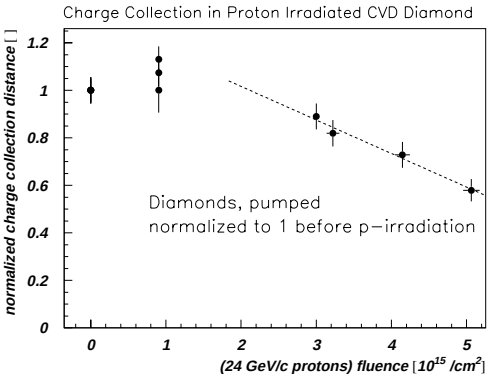

Figure 22: Charge collection distance on diamond samples as a function of the proton fluence. The charge collection distances on each sample are normalized to its (electron)pumped value before proton irradiation.

irradiation with 0.9×10^{15} p/cm^2 the pumped values are slightly increased compared to before proton irradiation. The next measurement at 3×10^{15} p/cm^2 shows a decrease by 10% compared to before proton irradiation. Measurements on the other samples at higher fluence show a decreasing charge collection distance. A linear fit to the values above 3×10^{15} p/cm^2 intersects the ordinate value one at a fluence of $\approx 2 \times 10^{15}$ p/cm^2. Charge collection distance normalized to the pumped value before proton irradiation appears to decrease linearly above $\approx 2 \times 10^{15}$ p/cm^2 and reaches 60 % of its unirradiated value at 5×10^{15} p/cm^2. As noted earlier the decrease of the most probable value is 20% at a fluence of 5×10^{15} p/cm^2. No decrease in charge collection distance below 1×10^{15} p/cm^2 is observed and we therefore conclude that CVD diamond is radiation hard up to at least 1×10^{15} protons/cm^2.

Fig. 23 shows the proton flux, as measured by the secondary emission chamber, and current measured on a diamond during the the first 55 hours of the proton irradiation. Protons were only

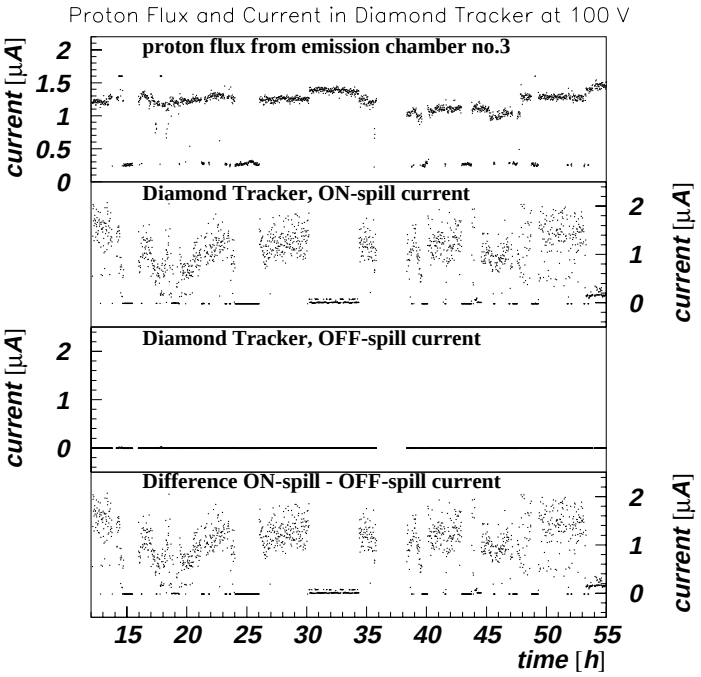

Figure 23: Proton flux as measured by the secondary emission chamber and current on a 2.9 mm^2 pad on the diamond strip detector during proton irradiation. The thickness of the diamond detector is 490 μm. The current was measured ON- and OFF-spill.

present during a spill of 300 ms. In this time the ON-spill current and the proton flux could be measured. The OFF-spill current was measured in breaks between spills. The difference between the ON- and OFF-spill current is the particle induced current. This current correlates with the proton flux. The OFF-spill current shown on the same scale as the ON-spill current is negligibly small. It remains constant during irradiation for all samples. The graph also shows that the induced current in diamond does not change with time and proton fluence which reached 1×10^{15} p/cm^2 [see Fig. 20] after 70 hours. At some points the induced current is low although protons were present (e.g. from 30 h to 35 h). This happened because beam steering magnets changed temporarily and shifted the beam spot by several milimeters to essentially miss the detectors.

5.1.2 Pion Irradiation

CVD diamond detector samples were irradiated with pions in four separate exposures since 1994 [13] including the recent irradiation at the end of 1997. All irradiations were performed at the PSI, Villingen, Switzerland. The pions had a momentum of 300 MeV/c, which is at the peak of the Δ resonance where the nuclear interaction cross-section between π^+ and protons inside the carbon nuclei reaches a maximum. The available pion flux on the samples was $\mathcal{O}(1.5 \times 10^9)$ $\pi/\mathrm{cm}^2/\mathrm{s}$. During irradiation the samples were kept at room temperature and biased with a voltage of 100 V or above. The highest accumulated pion fluence on samples was 1.8×10^{15} π/cm^2 at the end of the 1997 irradiation.

Fig. 24 shows a charge signal distribution measured on a diamond sample at different pion fluences. At a fluence of 1.8×10^{15} π/cm^2 the mean signal decreases by 15 %; the most probable signal remains constant. Such variation is close to the measurement error, especially when the measurements are separated in time. Fig. 25 shows the charge signal distribution on another sample before irradiation. After irradiation with 1.1×10^{15} π/cm^2 the charge collection distance is decreased by about 30 %. The same figure shows that the most probable value of the distribution remains nearly constant. The decrease of the mean signal is due to fewer entries in the tail of

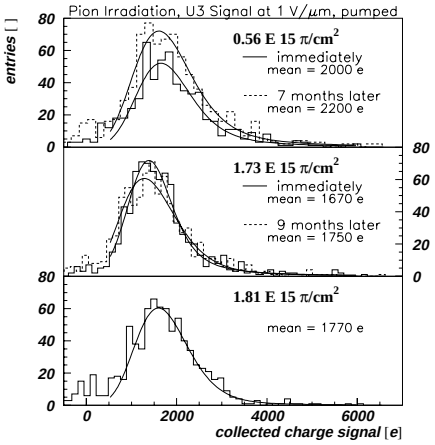

Figure 24: Charge signal distribution on a diamond sample with 55 μm charge collection distance before irradiation and after 1.8×10^{15} π/cm^2.

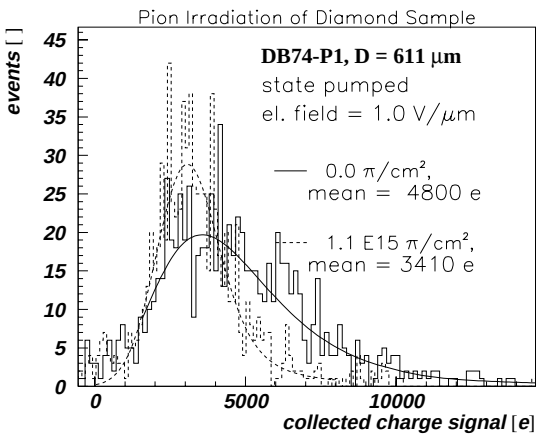

Figure 25: Charge signal distribution on a diamond sample with 133 μm charge collection distance before irradiation and after 1.1×10^{15} π/cm^2.

the Landau distribution. The normalized charge collection distance measured on all diamond samples after irradiation with pions is summarized as a function of pion fluence in Fig. 26. The

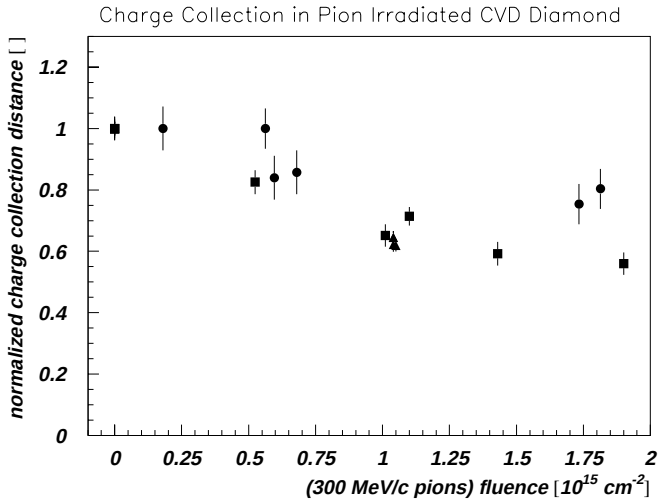

Figure 26: Charge collection distance on diamond samples as a function of the pion fluence. The charge collection distances on each sample are normalized to its (electron)pumped value before pion irradiation.

charge collection distance is normalized to the pumped state of the sample before irradiation. It is important to notice that this plot is based on a characterization of the mean value of collected charges. The most probable value decreases by less than 15 %. The dark current was measured before and after irradiation and decreases slightly after irradiation.

5.1.3 Neutron Irradiation

CVD diamond samples and silicon diodes were irradiated with neutrons in five exposures since January 1995 including the recent irradiation in December 1997. All irradiations took place at the ISIS facility at the Rutherford Appleton Laboratory, England. Both thermal neutrons with kinetic energies below 10 keV and neutrons with energies peaking at 1 MeV were available [14]. The mean neutron flux above 10 keV was about $(1.7 \pm 0.6) \times 10^8$ $n/\mathrm{cm}^2/\mathrm{s}$. The samples were generally irradiated at room temperature with a voltage of 100 V applied. In the last irradiation one diamond sample and two silicon diodes were irradiated at -8 °C.

Fig. 27 shows the measured charge signal distribution on a diamond sample before irradiation and after two neutron irradiations with the respective accumulated fluences up to 1.35×10^{15} n/cm^2. At a fluence of 0.75×10^{15} n/cm^2 the mean value on this sample is decreased by ≈15 %. The most probable value is unchanged. At a fluence of 1.35×10^{15} n/cm^2 the mean value is decreased by about 40 %. Fig. 28 shows the currents from a silicon diode kept at -8°C and two diamond sample kept at $+18$°C as a function of time during the irradiation. One diamond was located close to the spallation source and received 1 MeV neutrons

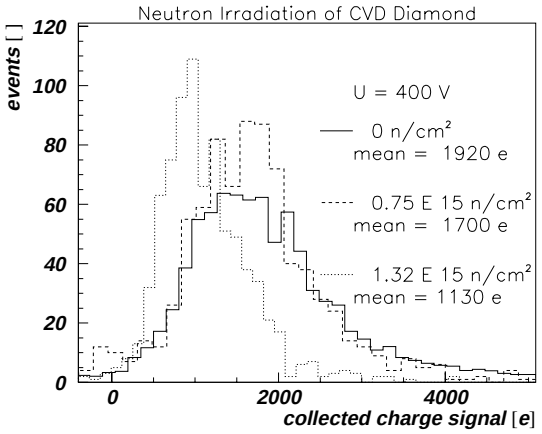

Figure 27: Charge signal distribution in a diamond sample before irradiation and after two neutron irradiations with the respective accumulated neutron fluence.

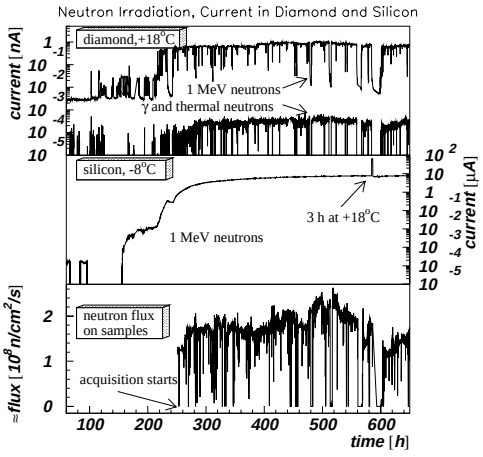

Figure 28: Neutron induced current during irradiation in diamond and a silicon diode for comparison.

and thermal neutrons. The other diamond was located far from the source and received thermal neutrons only. The induced current in diamond is several hundred pA when the beam is on and neutrons are present. The current correlates with the neutron flux which is shown as well. At constant neutron flux, the induced current remains constant over the entire irradiation. The current decreases by a factor of 100 during beam-off periods. The diamond sample shows a prompt response when beam returns. The sample which is exposed to 1 MeV neutrons shows an induced current which is higher by three orders of magnitude compared to the sample which receives thermal neutrons only. This is due to presence of photons associated with neutrons or to inelastic interactions of neutrons with carbon or hydrogen in the detector. The behaviour of the diamond is contrasted by the current in the silicon diode which shows a non-linear increase from a few pico Ampere to 10 μA after 600 hours. During beam-off periods the silicon current decreases due to annealing. The current in silicon increased by factor 10 during a 3 hours warm-up. However, when cooled again to -8°C, the current recovers to the value of before warm-up.

6 Proposed Research Program for 1998/1999

Although tremendous progress has been made in the past year there remains a coherent set of detector R&D tasks to complete the work of the RD42 project over the next year.

The main focus of our work will be the study of strip and pixel tracking devices. In particular we are studying the charge collection mechanism, are working on improving the spatial resolution and studying the material uniformity. In addition we will continue our material studies working with manufacturers to achieve 300 μm or higher charge collection distance diamond samples which are typically 400 μm thick. We will also work with manufacturers in scaling up production to produce large area low cost material for LHC experiments.

The diamonds we have now have most probable signals of 6000 e. With the electronics we have developed in the DMILL process with Matra-MHS over the last year we should soon achieve better than 10:1 signal to noise with electronics developed in a rad-hard technology. Having just received these chips we will mount them on the highest quality CVD material and test the first prototype in the coming months. We anticipate that it should be possible to build a demonstrator rad-hard, CVD diamond strip module with a significant area (2×4 cm^2) by the end of the upcoming year. Such a device would be guaranteed to survive the full life of the LHC at the inner strip radii in either ATLAS or CMS and as such could prove very interesting for either of these experiments. There remains the task of building, irradiating and testing detector prototypes.

We have begun a programme of generic pixel sensor R&D. We are actively working with both CMS and ATLAS to find a metallization and bump-bonding solution for sensors based on CVD diamond. We anticipate that this work will continue at least over the next year. At this stage we are making tremendous headway by exploring all possibilities simultaneously. Eventually it may be more appropriate that this work continue under the auspices of the individual experiments, but until there are a number of bonding alternatives commercially available it seems more appropriate for this work to continue as a generic R&D.

We have demonstrated that we are now in the position to create the first full size, radiation hard LHC tracking detectors which will perform with more than $10:1$ signal to noise at LHC shaping times and will last for more than ten years of trouble free LHC operation at small radii. In addition to this we are in a position to make the first fully efficient bump-bonded pixel tracker prototypes suitable for use in the vertex regions of ATLAS or CMS.

We believe that the RD42 collaboration can most effectively do the specific prototyping work for each of the proposed LHC experiments. A fragmentation of this effort into the different experiments at this stage would be an enormous setback. We do, however, see this work will naturally evolve into an experimental design over the next 12 to 18 months.

7 Responsibilities and Funding for 1998/1999

What follows is a breakdown of the areas of research that will be pursued at the different institutes (Table 2) involved in the project, a budget for the work to be carried out (Table **??**) and sources of funding expected for the project (Table **??**).

7.1 Requests from CERN Infrastructure

It is anticipated in addition to the funding needed to purchase diamond samples and develop radiation hard low noise electronics, that the following requests will be made on the CERN infra-structure:

- four 5-day testbeam running periods per year for the duration of the project;
- computing time and disk space on the central CERN computers;
- maintain the present 20 m^2 of laboratory space for test setups, detector preparation and electronics development;
- maintain the present office space for full time residents and visiting members of our collaboration;

7.2 Research Responsibilities

	Diamond Characterization	Meeting with Companies	Radiation Hardness	Detector Design LHC	Detector Design Heavy Ion	Detector Design other	Rad-Hard Electronics	Data Analysis	Material Studies	Diamond Growths
Vienna			x					x		
MPIK-HD	x		x							
GSI	x				x				x	
LETI/CEA	x								x	x
LENS									x	
Univ. Florence	x								x	x
LEPSI/CNRS	x		x	x			x			
Rutgers	x		x					x		
CERN	x	x	x	x			x	x	x	
CPPM							x			
LEPES									x	
NIKHEF	x							x		
Univ. Torino	x								x	
OSU	x	x	x					x	x	
Bristol			x							
Hamburg	x								x	
Pavia							x			
FNAL								x		
IHEP, Bern	x					x			x	
Univ. Melbourne	x									
CMU	x					x			x	
UTO	x	x						x		
IIT						x				
LANL			x							

Table 2: Research interests of groups involved in RD42.

7.3 Funding Request

this page is void in this version of the report

8 Publications and Talks given by RD42

8.1 Publications since 1996

1. W. Adam *et al.*, "Radiation Hardness Studies of CVD Diamond Detectors", Nucl. Instr. and Meth. **A367** (1996) 207.

2. W. Dulinski *et al.*, "Results from CVD Diamond Trackers", Nucl. Instr. and Meth. **A367** (1996) 212.

3. C. Bauer *et al.*, "Pion Irradiation Studies of CVD Diamond Detectors", CERN-PPE/95-173, (1995).

4. C. Bauer *et al.*, "Recent results on chemical-vapor-deposited diamond microstrip detectors", Nucl. Instr. Meth. **A380** (1996) 183.

5. C. Bauer *et al.*, "Recent results from the RD42 diamond detector collaboration", Nucl. Instr. Meth. **A383** (1996) 64.

6. D. Meier *et al.* (RD42-Collaboration), "Diamond as a Particle Detector", It. Phys. Soc. **52** (1996) 105.

7. M.M. Zoeller *et al.*, "Performance of CVD Diamond Microstrip Detectors under Particle Irradiation", IEEE Trans. Nucl. Sci. **44** (1997) 815.

8. W. Adam *et al.* (RD42 Collaboration), "Development of CVD Diamond Radiation Detectors", CERN-EP/98-80, in Proc. of 5^{th} Symposium on Diamond Materials, Electrochemical Society, Paris, (1997).

9. M. Krammer *et al.* (RD42 Collaboration), "Development of CVD Diamond Radiation Detectors" in Proc. of VERTEX 97, Rio de Janeiro, (1997)

10. W. Trischuk *et al.* (RD42 Collaboration), "Semiconductor Trackers for Future Particle Physics Detectors", in Proc. of Vienna Wire Chamber Conference, Vienna, (1998).

11. E. Berdermann *et al.*, "Diamond Detectors for Heavy Ion Measurements at GSI Darmstadt", Nucl. Instr. Meth. **B61** (1998) 399.

12. D. Meier *et al.* (RD42 Collaboration), "Proton Irradiation of CVD Diamond Detectors for High Luminosity Experiments at the LHC", CERN-EP/98-79, in Proc. of 2^{nd} Int. Conf. Radiation Effects Semiconductor Mat., Detectors and Devices, Florence (1998).

13. W. Adam *et al.* (RD42 Collaboration), "CVD Diamond Microstrip Detectors", in Proc. of 2^{nd} Int. Conf. Radiation Effects Semiconductor Mat., Detectors and Devices, Florence (1998).

14. W. Trischuk *et al.* (RD42 Collaboration), "Bump Bonded Pixel Detectors on CVD Diamond from RD42", in Proc. of Int. Pixel Workshop, FNAL, (1998).

15. R. Stone *et al.* (RD42 Collaboration), "Radiation Hardness of CVD Diamond Detectors", in Proc. of Int. Pixel Workshop, FNAL, (1998).

8.2 Talks since 1996

1. EuroDiamond 96, Torino 1996
2. First Int. Conf. on Radiation Effects on Semiconductor Material, Detectors and Devices, Florence 1996 (2 talks)
3. 5^{th} Workshop on GaAs and Related Materials, Glasgow 1996
4. Vertex 96, Chia 1996
5. 5^{th} Int. Conf. on Advanced Technology and Particle Physics, Como 1996 (4 talks)
6. IEEE 96, Taos 1996
7. VHLC Workshop, FNAL 1997
8. Elba 97, Elba 1997
9. 2^{nd} Int. Conf. on CP Violation, Honolullu 1997
10. Vertex 97, Rio de Janeiro 1997
11. 5^{th} Symp. on Diamond Materials, Paris 1997
12. EPS 97, Jerusalem 1997
13. 3^{rd} Int. Meeting on Front-End Electronics for High Resolution Tracking Detectors, Taos 1997
14. 3^{rd} Int. (Hiroshima) Symposium on the Development and Application of Semiconductor Tracking Detectors, Melbourne 1997
15. Vienna Wire Chamber Conference, Vienna 1998
16. 2^{nd} Int. Conf. on Radiation Effects in Semiconductor Materials, Detectors and Devices, Florence, 1998 (2 talks)
17. Pixel 98, FNAL 1998 (2 talks)

References

[1] W. Adam *et al.* (RD42-Collaboration). "Development of Diamond Tracking Detectors for High Luminosity Experiments at the LHC". Status Report/RD42, CERN, (Jan. 1997). LHCC 97-3.

[2] IDEAS Company. "The VA Circuits". *Catalogue*, 95/96.

[3] M. Turala. "PPE-News, LHCC Section", (March 13/14, 1997).

[4] LHC Committee. "Minutes of the 27^{th} meeting of the LHCC", (1997). CERN/LHCC 97-28.

[5] C. Colledani *et al.* "A Submicron Precision Silicon Telescope for Beam Test Purposes". *Nucl. Instr. Meth.*, **A372** (1997) 3.

[6] E. Belau *et al.* "Charge Collection in Silicon Strip Detectors". *Nucl. Instr. Meth.*, **214** (1983) 253-260.

[7] F. Anghinolfi *et al.* "SCTA - A Radiation Hard BiCMOS Analogue Readout ASIC for the ATLAS Semiconductor Tracker". *IEEE Trans. Nucl. Sci.*, **44** (1997) 3.

[8] ATLAS Collaboration. "Inner Detector Technical Design Report", (1997). CERN/LHCC/97-17.

[9] CMS Collaboration. "CMS Tracker TDR 5", (1998). CERN/LHCC 98-6.

[10] M.H. Nazaré *et al.* (RD42-Collaboration). "Development of Diamond Tracking Detectors for High Luminosity Experiments at the LHC". RD42-Proposal, CERN, (May 1994). DRDC 94-21/P56.

[11] W. Dulinski. "Electron Irradiation of CVD Diamond". RD42 Collaboration Meeting Notes, (June 1995).

[12] D. Meier *et al.* (RD42-Collaboration). "Proton Irradiation of CVD Diamond Detectors for High Luminosity Experiments at the LHC". ., 2^{nd} Int. Conf. Radiation Effects Semiconductor Mat., Detectors and Devices, Florence, Preprint CERN-EP/98-79, (1998).

[13] C. Bauer *et al.* (RD42-Collaboration). "Pion Irradiation Studies of CVD Diamond Detectors". Preprint CERN-PPE/95-173, (1995).

[14] M. Edwards and D.R. Perry. "The Radiation Hardness Test Facility". *RAL Report*, RAL-90-065, (1990).